Structure of force networks in tapped particulate systems of disks and pentagons. II. Persistence analysis

L. Kondic,[1] M. Kramár,[2] Luis A. Pugnaloni,[3,4] C. Manuel Carlevaro,[5,6] and K. Mischaikow[2]
[1]*Department of Mathematical Sciences, New Jersey Institute of Technology, Newark, New Jersey 07102, USA*
[2]*Department of Mathematics, Rutgers University, Piscataway, New Jersey 08854-8019, USA*
[3]*Dpto. de Ingeniería Mecánica, Facultad Regional La Plata, Universidad Tecnológica Nacional, Av. 60 Esq. 124, 1900 La Plata, Argentina*
[4]*Consejo Nacional de Investigaciones Científicas y Técnicas, Argentina*
[5]*Instituto de Física de Líquidos y Sistemas Biológicos (CONICET La Plata, UNLP), Calle 59 Nro 789, 1900 La Plata, Argentina*
[6]*Universidad Tecnológica Nacional-FRBA, UDB Física, Mozart 2300, C1407IVT Buenos Aires, Argentina*
(Received 4 October 2015; published 14 June 2016)

In the companion paper [Pugnaloni *et al.*, Phys. Rev. E **93**, 062902 (2016)], we use classical measures based on force probability density functions (PDFs), as well as Betti numbers (quantifying the number of components, related to force chains, and loops), to describe the force networks in tapped systems of disks and pentagons. In the present work, we focus on the use of persistence analysis, which allows us to describe these networks in much more detail. This approach allows us not only to describe but also to quantify the differences between the force networks in different realizations of a system, in different parts of the considered domain, or in different systems. We show that persistence analysis clearly distinguishes the systems that are very difficult or impossible to differentiate using other means. One important finding is that the differences in force networks between disks and pentagons are most apparent when loops are considered: the quantities describing properties of the loops may differ significantly even if other measures (properties of components, Betti numbers, force PDFs, or the stress tensor) do not distinguish clearly or at all the investigated systems.

DOI: 10.1103/PhysRevE.93.062903

I. INTRODUCTION

In the companion paper [1], we compare the force networks in tapped systems by using relatively simple measures: probability density functions (PDFs) for normal and tangential forces between the particles, correlation functions describing positional order of the considered particles, as well as possible correlations of the emerging force networks. These classical measures are supplemented by analysis of cluster sizes and distributions at different force levels (i.e., by considering the part of the force network that only includes contacts involving forces exceeding a threshold). These results have uncovered some differences between the force networks in the considered systems. For example, we have found that the number of clusters as a function of the force level is heterogeneous in the tapped systems under gravity, with different distributions deeper in the samples compared to the ones measured closer to the surface. However, some of the differences remain unclear. For example, tapped disks exposed to different tap intensities that lead to the same (average) packing fraction are found to have similar PDFs and similar cluster-size distributions, although it is known [2] that there are some differences in the geometrical properties of the contact networks in these systems.

In the present paper, we focus on a different approach, based on persistence analysis. This approach has been successfully used to explain and quantify the properties of force networks in the systems exposed to compression [3–5]. In essence, persistence analysis allows us to quantify the force network "landscapes" in a manner that is global in character, but it still includes detailed information about the geometry at all force levels. The global approach to the analysis of force networks makes it complementary to other works that have considered in detail the local structure of force networks [6], and attention to geometry distinguishes this approach from network-type analysis [7–10]. We will use persistence analysis to compare the force networks between the systems of disks exposed to different tapping intensities, as well as to discuss similarities and differences between the systems of disks and pentagons. As we will see, some differences between the considered networks that could not be clearly observed (and even less quantified) using classical measures become obvious when persistence analysis is used. Since properties of the force networks are related to the macroscale response of the systems, such as conductivity and sound propagation, persistence analysis predicts that the macroscale response of the systems considered will differ as well. Furthermore, persistence analysis allows for formulating measures that can be used to quantify, in a precise manner, differences in force networks between realizations of a nominally same system. We note that persistence has been used to quantify the features in other physical systems such as isotropically compressed granular media [3–5], where it was shown based on persistence analysis that it was possible to quantify the influence of friction on the force networks properties. Persistence was also used to study dynamics of the Kolmogorov flow and Rayleigh-Bénard convection [11].

This paper is organized as follows. In Sec. II, we discuss briefly the persistence approach and also provide some examples to illustrate its use in the present context. In Sec. III, we discuss the outcome of persistence approach and quantify the differences between the considered systems. Section IV is devoted to the conclusions and suggestions for the future work.

II. METHODS

A. Simulations

The simulations utilized in this paper are described in detail in Ref. [1]; here we provide a brief overview. We consider tapped systems of disks and pentagons in a gravitational

field. The particles are confined in a two-dimensional (2D) rectangular box with solid (frictionless) side walls. Initially, 500 particles are placed at random (without overlaps) into the box, and the particles are allowed to settle to create the initial packing. Then, 600 vertical taps are applied to each system considered; we discard the initial 100 taps and analyze the remaining 500. After each tap, we wait for the particles to dissipate their kinetic energy and achieve a mechanical equilibrium. We record the particles positions and the forces acting between them; the interactions between the particles and the walls are not included. For more direct comparison, the forces are normalized by the average contact force.

In addition to discussing the influence of particle shape, we consider two different tapping intensities, Γ (called "high" and "low" tap in what follows), which lead to the same packing fractions for disks [$\Gamma = 3.83\sqrt{dg}$ (low) and $\Gamma = 12.14\sqrt{dg}$ (high), where d is the disk radius and g the acceleration of gravity]. We also discuss the influence of gravitational compaction, and for this purpose we consider "slices" of the systems, 10 particle diameters thick: bottom slice positioned deep inside the domain, and the top slice close to the surface. See Ref. [1] for more details.

B. Persistent homology

We are interested in understanding the geometry exhibited by force networks. Their complete numerical representation contains far too much information. With this in mind, we make use of the tools from algebraic topology, in particular homology, to reduce this information by counting simple geometric structures. In the two-dimensional (2D) setting of interest in the present context, fixing a magnitude, F, of the force and considering the particles that interact with a force at or above F yields a 2D topological space, $X(F)$. Two simple geometric properties of $X(F)$ are the number of components (clusters), $\beta_0(X(F))$, and the number of loops (holes), $\beta_1(X(F))$.

In Ref. [1] it is shown that even though we are counting very simple geometric objects, by varying the threshold F, the set of Betti numbers $\beta_0(X(F))$ and $\beta_1(X(F))$ provides novel distinctions between the behavior of the above-mentioned systems. However, there is an obvious limitation to just using the Betti numbers to describe a system. Consider two different thresholds and assume that the values of the Betti numbers are the same. Does this mean that the geometric structures, e.g., components and loops, are the same at these two thresholds, or have some components or loops disappeared and been replaced by an equal number of different components or loops? This distinction cannot be determined from the Betti number count alone.

To provide a more complete description, we make use of a relatively new algebraic topological tool called *persistent homology*. In the context of the 2D systems that we are considering here, it is sufficient to remark that to each force network landscape persistent homology assigns two *persistence diagrams*, PD_0 and PD_1, such as those shown in Fig. 1. Each persistence diagram consists of a collection of pairs of points $(b,d) \in \mathbb{R}^2$, where b, the birth, indicates the threshold value at which a geometric structure (a component and cluster for PD_0 or a loop for PD_1) first appears, and d, the death, indicates the threshold value at which the geometric structure disappears. In this paper we measure the geometry of the part of the contact network with force interactions greater than a given threshold, and thus $b \geqslant d$. The value $b - d$ is called the *lifespan*. Note that the component represented by the point (b,d) "dies" when it merges with some other component with the birth coordinate larger or equal to b. In particular, the single generator in PD_0 with death coordinate -1, see Fig. 1(a), represents the component that contains the strongest force "chain" in the system: the one that formed at the highest force level. Note that it has both the highest birth value and the longest lifespan. More detailed interpretation of PD_0 in 1D can be found in Ref. [4], while a rigorous presentation for 2D is given in Ref. [5].

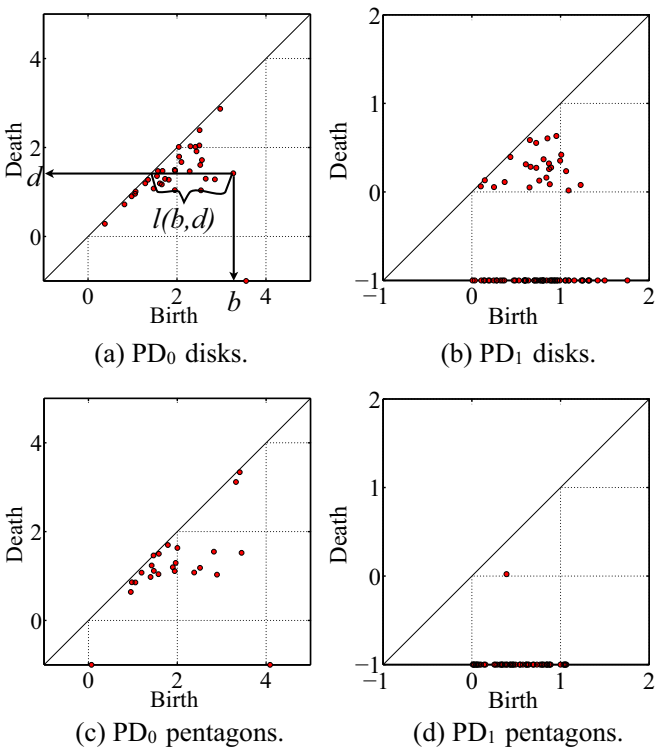

FIG. 1. Examples of PDs corresponding to the normal force network of one realization of systems of disks and pentagons (low tapping, bottom slice). In the part (a) we also illustrate some of the concepts that will be used later in the paper: b (birth time), d (death time), and $l(b,d)$ (lifespan).

The loop structure of a force network is described by PD_1. A loop in the network is a closed path of the edges connecting centers of the particles. Similar to PD_0, the point $(b,d) \in \mathsf{PD}_1$ indicates that a loop appears in the part of the network exceeding the force threshold b. This loop is present for all the values of the threshold in $(d,b]$. At the value d, this loop is filled in, that is, the interior of the loop is filled in with particles that form a crystalline structure, and the forces between the interacting particles inside of the loop are larger or equal to d. This fill-in process can be also seen as filling the loop by "trivial" loops formed by exactly three particles with forces stronger or equal to d. To visually distinguish the loops that do not get filled in at any force level (including the threshold 0), we set their death time to $d = -1$. However,

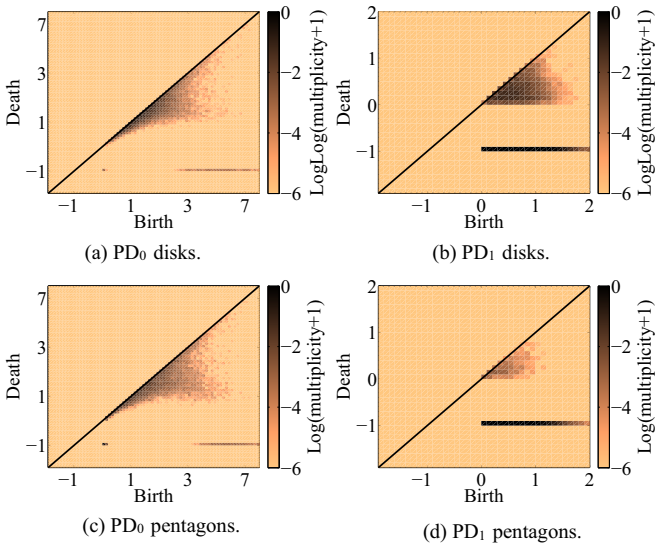

(a) PD_0 disks. (b) PD_1 disks.

(c) PD_0 pentagons. (d) PD_1 pentagons.

FIG. 2. Superimposed PDs for the normal force networks of disks and pentagons, including superimposed points from 500 realizations (bottom slice, low tapping).

in the distance computations (discussed below) we follow the convention presented in Ref. [5] and replace them by 0. Note that in the example shown in Fig. 1, for pentagons there is a single loop that gets filled in (close to threshold level 0), while for disks there is a number of loops that gets filled in at a variety of thresholds.

A particularly simple descriptor based on the lifespans is the total persistence, $\mathfrak{T}(\mathsf{PD}) = \sum_{(b,d)\in\mathsf{PD}}(b-d)$, i.e., the sum of all lifespans of the points in PD. In the context of Fig. 1, the total persistence of Figs. 1(a) and 1(c) is roughly the same, while the total persistence of Fig. 1(b) is roughly twice that of Fig. 1(d). Thus, this gives a simple measure that can, at least in some settings, distinguish persistence diagrams arising from different systems. To further distinguish the diagrams, we will also consider the distribution of lifespans (representing the number of times a value of lifespan in a specified range is found).

As is made clear in Sec. III, even within a single system there can be considerable variability in the force networks from tap to tap. Unfortunately, the concept of an average persistence diagram is not yet well defined [12–14]. However, using the above-mentioned measures we avoid this difficulty by applying them to an aggregate persistence diagram obtained by considering, as is done in Fig. 2, all persistence points from the 500 simulated taps on a single diagram. The distributions of birth times presented in Sec. III are based on these diagrams. Note that for the remainder of the paper the distributions of birth times and lifespans are *normalized by the number of particles* in the domain used to define the force network under consideration.

We note that the PDs provide a compressed and simplified description of the underlying force network landscape. Thus, some information, such as size, shape, and position of the components or loops, is discarded while passing from a force network to the corresponding PD. Therefore, different force networks may produce the same PDs. However, as is discussed in Sec. II C, there are metrics that can be imposed on the space of all persistence diagrams such that if two force network landscapes are similar, then their associated persistence diagrams are similar. On the other hand, if the diagrams differ considerably, then so do the corresponding force networks. Hence, in summary, persistent homology provides a continuous reduction of information that captures geometric information.

It is worth mentioning that persistence computations extend to higher dimensions. In particular, for 3D, the diagram PD_0 describes the structure of the connected components, as in 2D. The features in PD_1 are interpreted as tunnels rather than loops. Finally, there is an additional diagram PD_2 that describes the structure of cavities.

The computational codes used to construct the force networks and persistence diagrams are available at Refs. [15,16], respectively. There are also other publicly available packages for computing persistent homology [17].

C. Distance between persistence diagrams

In the previous section, we introduced specific descriptors of persistence diagrams based on a single feature of the points, e.g., lifespan or birth value. In this section we discuss metrics on the space of persistence diagrams that are based on the entire diagram; i.e., we compare two diagrams by comparing all points in each diagram. Note that this comparison does not involve force thresholding: this measure compares the force networks at all force levels.

Consider two persistence points $p_0 = (b_0,d_0)$ and $p_1 = (b_1,d_1)$. The distance between p_0 and p_1 is defined by

$$\|(b_0,d_0) - (b_1,d_1)\|_\infty := \max\{|b_0 - b_1|, |d_0 - d_1|\}.$$

Now, given two persistence diagrams PD and PD′ let $\gamma : \mathsf{PD} \to \mathsf{PD}'$ be a bijection between points in the two persistence diagrams where we are allowed to match points of one diagram with points on the diagonal of the other diagram. The *degree-q Wasserstein distance*, $d_{W^q}(\mathsf{PD},\mathsf{PD}')$, is obtained by considering for each bijection, γ, the quantity

$$\left(\sum_{p\in\mathsf{PD}} \|p - \gamma(p)\|_\infty^q\right)^{1/q},$$

and defining the distance between PD and PD′ to be the minimum value of this quantity over all possible bijections. Stated formally,

$$d_{W^q}(\mathsf{PD},\mathsf{PD}') = \inf_{\gamma:\mathsf{PD}\to\mathsf{PD}'} \left(\sum_{p\in\mathsf{PD}} \|p - \gamma(p)\|_\infty^q\right)^{1/q}.$$

The *bottleneck distance* $d_B(\mathsf{PD},\mathsf{PD}')$ is given by

$$d_B(\mathsf{PD},\mathsf{PD}') = \inf_{\gamma:\mathsf{PD}\to\mathsf{PD}'} \sup_{p\in\mathsf{PD}} \|p - \gamma(p)\|_\infty.$$

The cost of "moving the points" (i.e., selecting a given bijection) varies for different distances. The bottleneck distance captures only the largest move corresponding to the largest difference between the diagrams. On the other hand, the Wasserstein distance d_{W^1} sums up all the differences with equal weight. If all the points in one diagram are close to the

points in the other diagram (or close to the diagonal), then the bottleneck distance is small. However, d_{W^1} tends to be large since it is a sum over a large number of small differences. In the case that d_{W^1} is close to d_B the diagrams tend to differ in a small number of points. There is the following relation between the distances: $d_B \leqslant d_{W^p} \leqslant d_{W^1}$ for $p > 1$ and d_{W^p} converges to d_B as p goes to infinity. Hence, using the d_{W^2} distance keeps track of all the changes but the small differences contribute less. Comparing the d_B,d_{W^1} and the d_{W^2} distances allows us to better understand the difference between the diagrams. For example, if d_B and d_{W^2} are similar but d_{W^1} is large, then there is only one dominant difference between the diagrams and a large number of small differences.

To compare a large number of PDs representing the steady states of the tapped systems, we use the distance matrix (heat map) D. The entry $D(i,j)$ is the distance between the diagrams corresponding to the taps i and j. Clearly, $D(i,i) = 0$, and if the states are similar, then the value $D(i,j)$ is small. The distance matrix provides a detailed information about the differences between all the states. Sometimes a more condensed representation of the differences between the states is desirable; for this purpose we will use distribution of the values of D.

To illustrate that the distance matrices are sensitive to the structure of the force networks, and furthermore that they allow for a simple visual inspection of the similarities and differences both between the considered systems and between different realizations and taps for the same system, we provide here an example. We consider a system of disks exposed to high-intensity tapping, record all the force information, and then randomly mix up the forces. This randomization is done after each tap by performing 1000 force swaps (i.e., picking any two contacts at random and swapping the forces between them). This procedure leaves the PDFs of the force networks unchanged; however, the force network may undergo a dramatic change, since one expects the force chains to be broken into a large number of short chains and therefore the differences between the states should be larger.

Figure 3 shows the d_{W^1} distance matrix for the original and randomized system. Considering the distances between PD_0 diagrams first, we see that the distances between "real" realizations are small compared to the ones between randomized systems, and also that the distances between the original and randomized states are larger than the ones between the randomized states. On the contrary, the variation in PD_1 diagrams is smaller for the randomized systems. This is due to the fact that by randomly reassigning the forces, the loops with strong force interactions are destroyed and the points in PD_1 tend to be close to the diagonal.

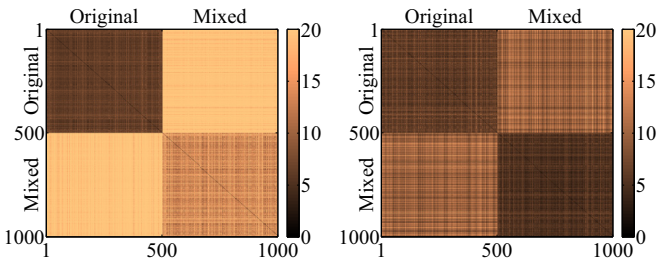

(a) PD_0 normal forces. (b) PD_1 normal forces.

FIG. 3. Distance matrices showing d_{W1} for randomly mixed-up forces between the particles (disks, bottom slice, high tapping). The axes show the number of tap and realization, and the colors illustrate the value of the distance.

We conclude that the distance matrices clearly identify the differences between original simulation results and the randomized ones. As we will see in what follows, they can be also used to identify the differences between various simulation results considered in the present work.

III. RESULTS

A. Influence of gravitational compaction on force network properties

Gravitational compaction and its influence on force networks is discussed in Ref. [1], where it is shown that PDFs of the normalized forces do not depend on the depth in the sample. However, using β_0 to count components shows differences: for both normal and tangential forces the number of components for the bottom slices is considerably larger than for the top ones. In this paper we compare top and bottom slices using the corresponding distance matrices and the descriptors discussed in the previous section.

Figure 4 shows the d_{W^1} distance matrices for the persistence diagrams of top and bottom slices of disks packings, respectively. While distances between the components do not appear to vary significantly, three observations can be made regarding PD_1 distances, shown in Figs. 4(c) and 4(d): (1) the distance between persistence diagrams of the top slice associated with different taps is relatively small (see lower right corners); (2) persistence diagrams of the bottom slice exhibit more variability (see upper left corners); and (3) the distances between persistence diagrams for different taps from the top slice and bottom slice range from small to large (see upper right corners). To reinforce these observations, we include

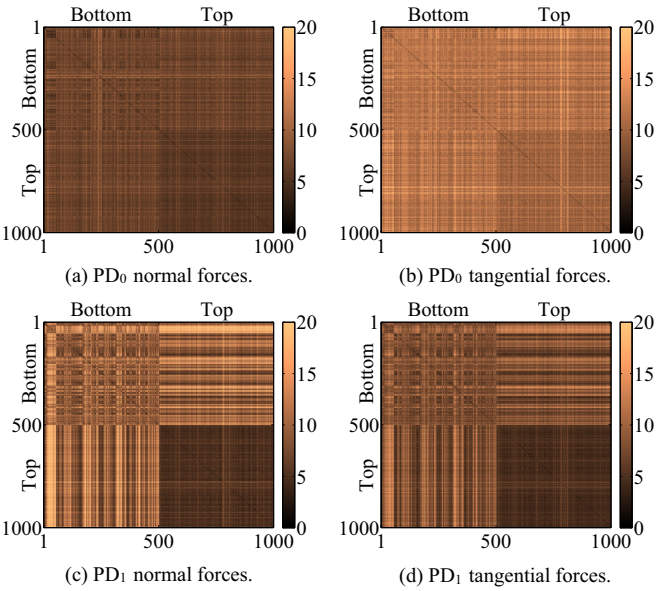

(a) PD_0 normal forces. (b) PD_0 tangential forces.

(c) PD_1 normal forces. (d) PD_1 tangential forces.

FIG. 4. Distance matrices showing d_{W1} (disks, low tapping).

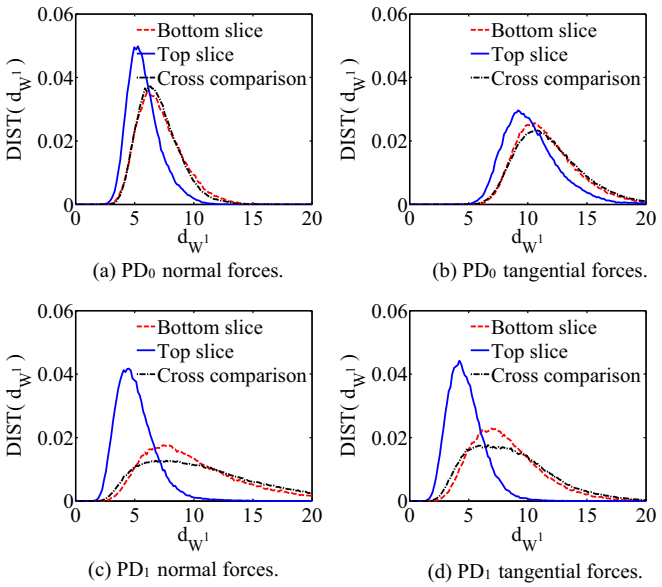

(a) PD_0 normal forces. (b) PD_0 tangential forces.

(c) PD_1 normal forces. (d) PD_1 tangential forces.

FIG. 5. Distributions of d_{W1} distance (disks, low tapping).

Fig. 5 that contains plots of the distribution of the distances. The distributions are computed only from the upper triangle of the distance matrix. Hence, the diagonal (zero) entries are not included. One immediate conclusion from observation (3) is that the geometry as measured by persistence diagrams for the force network observed after each tap for the top slice are not far away from those for the bottom slice, but lay on a small "subdomain" of this second more scattered set. Hence, the cross-comparison distances are dominated by the scattered distances of the bottom slice networks.

These distinctions are much less pronounced in Fig. 6, which shows d_B distance. This suggests that there is no single pronounced difference in the geometry of the force networks. In addition, d_{W^2} (picture not shown for brevity), turns out to

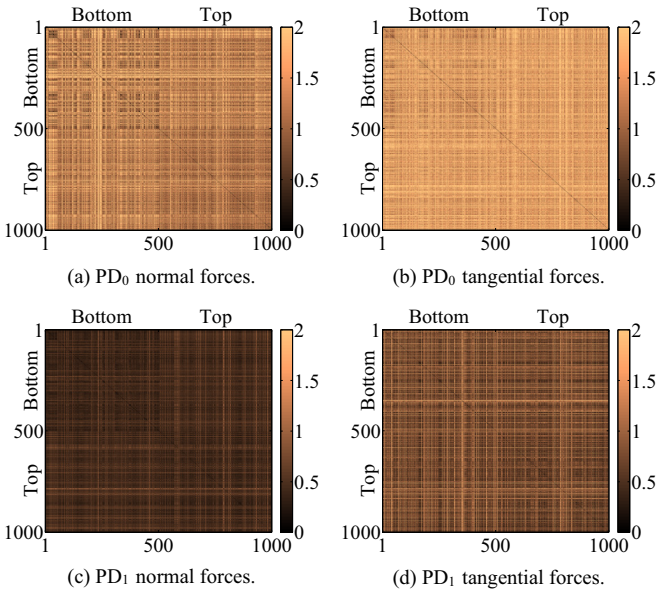

(a) PD_0 normal forces. (b) PD_0 tangential forces.

(c) PD_1 normal forces. (d) PD_1 tangential forces.

FIG. 6. Distance matrices showing d_B (disks, low tapping).

be quantitatively similar to the d_B distance matrices. Based on the discussion in Sec. II C, this fact indicates that the force networks for the bottom and top slices are similar, but the number of small variations in the birth and death of each feature (cluster or loop) from tap to tap are more prominent for the bottom slice. In particular, the light and dark bands of Figs. 4(c) and 4(d) suggest the existence of further structure in our systems that we explore in the next section.

Application of persistence analysis to the parts of the system exposed to different gravitational compaction, presented in this section, already illustrates the power of this approach: persistence provides detailed information not only about averaged properties of the force networks but also about their variability, which was not uncovered based on any of the approaches discussed so far. Since force network properties are closely related to the macroscale response, the prediction of this analysis is that fluctuations in the macroscale response will differ significantly for the parts of a sample exposed to different levels of gravitational compaction. We will see that similar conclusions can be also reached when comparing systems exposed to different tap intensities or systems with particles of different shape.

B. Force networks in the systems exposed to different tapping intensities

The measures considered in Ref. [1] (force PDFs, Betti numbers) do not identify differences in the properties of the force networks in the systems of disks exposed to different tapping intensities that lead to the same packing fraction. However, earlier work [2], based on different types of simulations where the side walls were frictional, which possibly influences the force network structure, suggested that some (rather difficult to observe) differences may exist. In this section we show that analysis based on persistent homology provides additional insight that allows us to understand the origin of the differences, both when considering averaged results and on the level of individual realizations and their variability.

Careful inspection of the distance matrices for different distance definitions, normal and tangential forces, components and loops, uncovers the following facts. First, we do not observe any appreciable differences between the distances when components and clusters are considered (figures not shown for brevity). Therefore, we expect that the distribution of components between the disk-based systems exposed to high and low tap intensities are similar (however see below). This conclusion does not apply to the distances between PD_1 diagrams. Figures 7(a) and 7(b) show the corresponding results for d_{W1} distance. There is a clear difference between high and low-tapping regimes, suggesting that the structure of the loops is very different. Figures 7(c) and 7(d) show the corresponding distributions confirming a clear separation between the two cases considered. In comparison to low-tapping states, high tapping is characterized by force networks that are significantly more similar to each other, both for normal and tangential forces. We emphasize that this difference is difficult to observe and quantify by using any other measure we are aware of. We also observe in Figs. 7(c) and 7(d) that the distances between the realizations for low tapping are as large as the distances

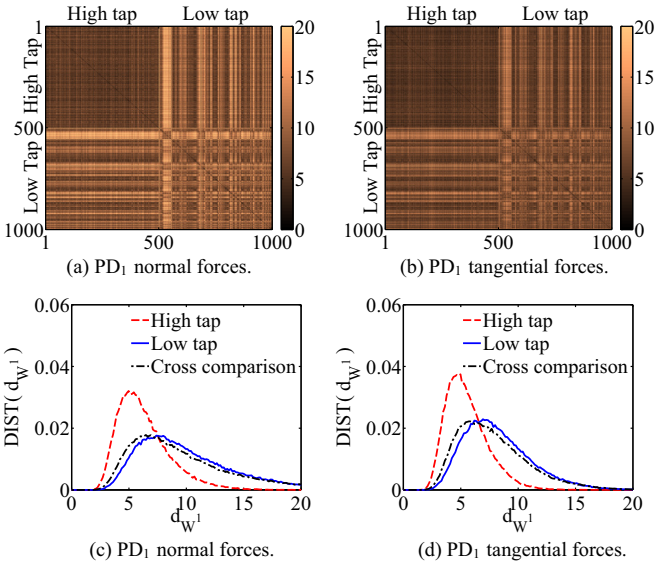

(a) PD_1 normal forces. (b) PD_1 tangential forces. (c) PD_1 normal forces. (d) PD_1 tangential forces.

FIG. 7. Distance matrices and distributions showing d_{W1} (disks, bottom slice).

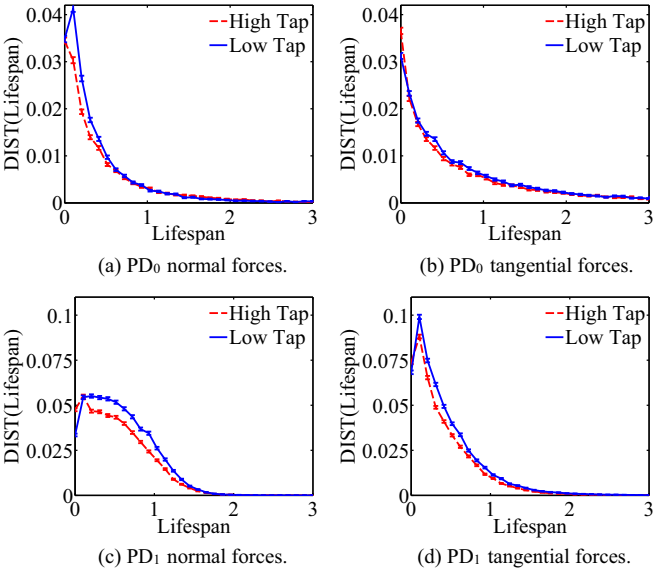

(a) PD_0 normal forces. (b) PD_0 tangential forces. (c) PD_1 normal forces. (d) PD_1 tangential forces.

FIG. 9. Distribution of lifespans (disks, bottom slice).

between low- and high-tapping regimes; we will discuss this finding in more detail in what follows.

We now proceed to answer the following two questions: (i) What is the difference between the structure of the networks for high and low tapping? (ii) Figures 7(a) and 7(b) show that there appears to be some structure in the evolution of the distances for PD_1 persistence diagrams. What is the origin of this structure?

To answer the first question, we now consider other measures that can be computed from PDs, starting with birth times. Figure 8 shows the distribution of birth coordinates for the considered PD_0 and PD_1 persistence diagrams. As a reminder, birth time indicates at what force threshold level the considered features (components, loops) appear. Perhaps

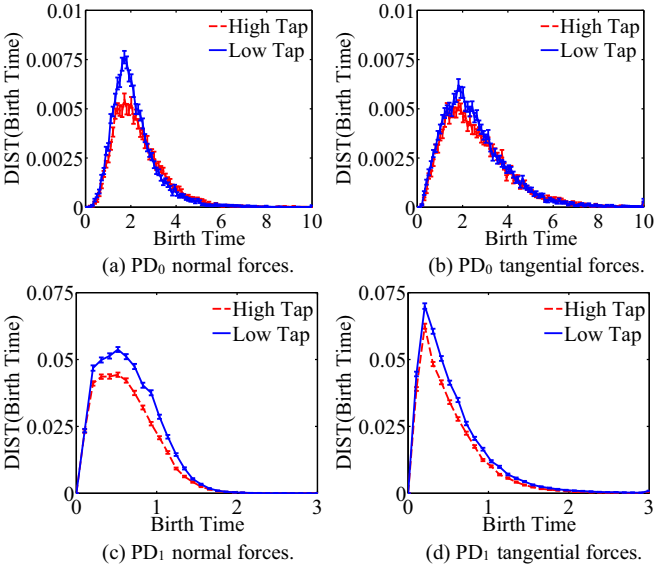

(a) PD_0 normal forces. (b) PD_0 tangential forces. (c) PD_1 normal forces. (d) PD_1 tangential forces.

FIG. 8. Distribution of birth times (disks, bottom slice). Only the features with the lifespan larger than 0.1 are included.

surprisingly, we see that not only the structure of loops is different, but the structure of components differs as well: for low-tapping regime, there is a much more pronounced peak, particularly for the normal forces. While consistent difference was seen when β_0 was considered (see Fig. 9 in Ref. [1]), the difference is more pronounced when considering birth times.

Figure 8 shows that in general there are more features born at every force level for low-tapping regime. In principle, it could happen that the lifespans of these extra features are relatively small and the systems only differ in minor fluctuations. Distributions of lifespans, shown in Fig. 9, demonstrate that this is not the case. The distributions of lifespans for low-tapping regime are typically above the distributions for the high-tapping regime. Therefore, even the number of prominent features is typically larger for the low-tapping regime. However, there is an important exception. For normal forces the number of components with a lifespan larger than one is larger for the high-tapping regime. The crossover of the PD_0 distributions for the normal force around the lifespan equal to one leads to the fact that the corresponding distributions of total persistence, shown in Fig. 10(a), are centered at the same point. As expected, the remaining distributions for the low-tapping regime, shown in Fig. 10, are shifted to the left.

While the interpretation of the results, such as the differences of birth times and lifespans, may not be immediately obvious, these measures show clearly the ability of the persistence analysis to distinguish between the considered systems. On a practical side, the fact that the differences *can* be identified suggests that the considered systems have different macroscopic properties.

So far, we have discussed one of the questions listed above, regarding the differences between the considered systems. Now we proceed to discuss the second one related to the origin of the structure apparent in Fig. 7 for the low-tapping regime. Recall (see Ref. [1], Sec. III B) that low tap intensity often does not lead to significant changes of the packings of disks from one tap to the next. Therefore, one may expect that

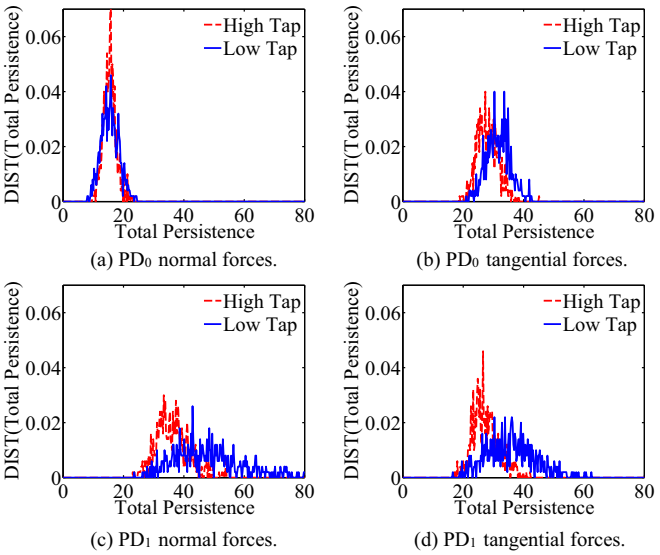

(a) PD_0 normal forces. (b) PD_0 tangential forces.

(c) PD_1 normal forces. (d) PD_1 tangential forces.

FIG. 10. Total persistence (disks, low tapping).

for a certain number of taps, the realizations are correlated, close to each other (with small distances between them), until the configuration of the particles, and the corresponding force network, change dramatically. The question is whether these "jumps" from one set of similar packings to another one are captured by the PDs.

To show that the answer to this question is positive, we recall that the packing fraction ϕ may change from one tap to the next. Since ϕ values obtained for different taps provide a rather noisy signal, we consider instead its auto-correlation function, as well as instantaneous cross-correlation between ϕ and total persistence, $\mathfrak{T}$ (for simplicity, we consider here $\mathfrak{T}$ instead of the distances). Regarding total persistence, we focus on $\mathfrak{T}(\mathsf{PD}_1)$. Figure 11 gives the results for the auto-correlation functions defined for any descriptor f as $c(t) = c(0)^{-1}[\langle f(0)f(t)\rangle - \langle f\rangle^2]$, where $\langle\rangle$ indicates an average over all time origins, and $c(0)$ is used to normalize so that $c(t=0) = 1$. Auto-correlation curves for ϕ show that while for high tapping there is no observable correlation between taps, for low tapping there is a clear correlation for up to 10–15 taps. This correlation is consistent with the structure of the distance matrices for low tapping; see Figs. 7(a) and 7(b). The results for $\mathfrak{T}(\mathsf{PD}_1)$ auto-correlation functions are very similar. We can go further

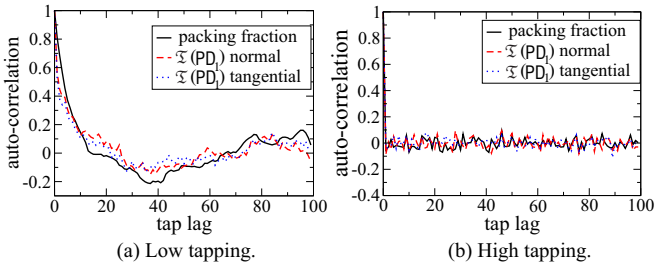

(a) Low tapping. (b) High tapping.

FIG. 11. Auto-correlation functions for (a) low and (b) high tapping. Each figure shows auto-correlation functions for packing fraction, ϕ, and total persistence, $\mathfrak{T}(\mathsf{PD}_1)$, for normal and tangential forces (disks, bottom slice).

and compute the instantaneous cross-correlation c between $\mathfrak{T}(\mathsf{PD}_1)$ and ϕ, defined as

$$c = \frac{\langle[\phi(t) - \langle\phi\rangle][\mathfrak{T}(\mathsf{PD}_1)(t) - \langle\mathfrak{T}(\mathsf{PD}_1)\rangle]\rangle}{\sigma_\phi \sigma_{\mathfrak{T}(\mathsf{PD}_1)}},$$

where σ indicates the variance of the variable. We find some degree of correlation between these two quantities: $c_{\phi\mathfrak{T}(\mathsf{PD}_1)}$ reaches the values of $\approx$0.6–0.7 for normal and tangential forces (here 1 means perfect correlation and 0 lack of correlation).

To rationalize the correlation of ϕ and $\mathfrak{T}(\mathsf{PD}_1)$, we recall the results obtained by considering the systems of disks exposed to compression [3]. In that system it was found that for monodisperse disks, which are more likely to crystallize (therefore having larger ϕ), there is a larger number of points in PD_1, consistent with the results presented here. We note that in Ref. [3] it was found that a larger number of points in PD_1 occurred for strong forces (with the idea that strong loops form at the boundaries of the fault zones separating crystalline regions); we expect a similar reason for the larger values of $\mathfrak{T}(\mathsf{PD}_1)$ in the present setting.

To conclude this section, we note that persistence analysis allows us to clearly identify differences between the systems of disks exposed to different tapping intensities leading to the same (average) packing fraction: these differences are particularly clear when considering the structure of loops. The differences are apparent for the averaged persistence diagrams but they are even more prominent when considering individual taps and their variability. This variability is much stronger for the systems exposed to low tapping. As already noted in the context of the results shown in Figs. 7(c) and 7(d), the differences between different realizations for low tapping may be as large as the differences between low- and high-tapping ones.

C. Force networks in the systems of disks and pentagons

In Ref. [1] we discussed some of the differences in the structure of the force networks between disks and pentagons. The main findings reported in that paper are that the differences between these systems manifest themselves particularly in the structure of tangential force networks measured by β_0 (although PDFs of the forces are almost indistinguishable), and by the number of loops, measured by β_1, for both normal and tangential forces. The number of loops in the disk-based system is consistently larger. This finding supports the idea that the clusters are larger for disks and therefore can support larger number of loops. In the present work, we will discuss additional insight that can be reached by persistence analysis.

Figures 12 and 13 show the distance matrices and corresponding distributions comparing disks and pentagons exposed to the same (low-) tapping intensity. In agreement with the results from Ref. [1], the differences between the components [the parts (a) and (b) of Figs. 12 and 13] are relatively minor. Considering loops, these figures show that the distances between pentagon-based systems are much smaller than for the disk-based ones. In particular, Fig. 13 shows that the distances between pentagon-based systems are centered at much smaller values, and their distribution is much narrower than for disks. We also note that the distances between disks and pentagons are much larger than between different

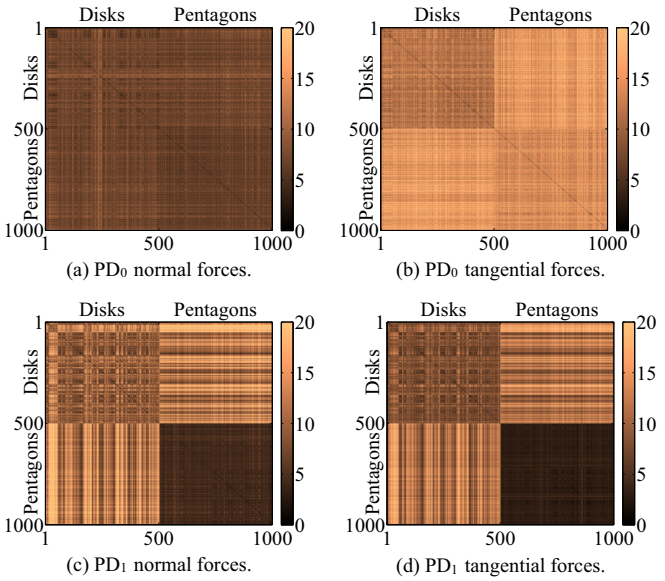

FIG. 12. Distance matrices showing d_{W1} (bottom slice, low tapping).

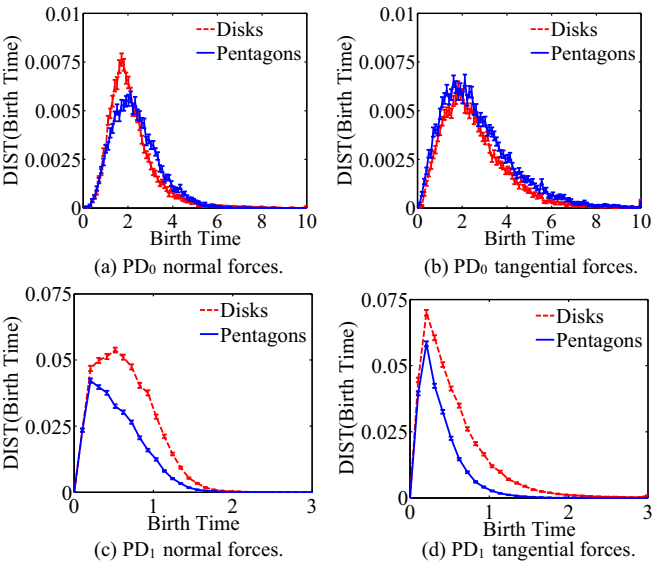

FIG. 14. Distribution of birth times (bottom slice, low tapping). Only the features with the lifespan larger than 0.1 are included. Compare to Fig. 15.

disk realizations, showing that persistence analysis clearly distinguishes these systems.

We note that consideration of other distances, such as bottleneck, d_B, that measures only the largest difference, are consistent with the ones presented for d_{W^1} distance (figures not shown for brevity). In particular, the distributions of d_B for loops are similar to the ones shown in Fig. 13, with the maximum and the spread for pentagons smaller than for disks. This is as expected, since the loops form at lower force level in pentagon-based system; compare Figs. 2(c) and 2(d).

We proceed by discussing the source of the differences between the disk- and pentagon-based systems considered so far. First, we focus on the distributions of birth times. Figures 14 and 15 show the corresponding results. The only difference between these figures is that in Fig. 14 we consider only the points with the lifespan larger than 0.1, while in Fig. 15 we consider all the points. The reason for showing both figures is that the differences between the two provide additional information about the points with short lifespan. Considering components for normal forces, parts (a) in these two figures, we observe that birth times capture some differences between the two systems that were not obvious when considering distances. There are more points in PDs for disks that are born around $F \sim 2$, and more points in PDs for pentagons born at larger forces. This is consistent with the PDFs for disks and pentagons shown in Fig. 10 of Ref. [1]. For the tangential forces, parts

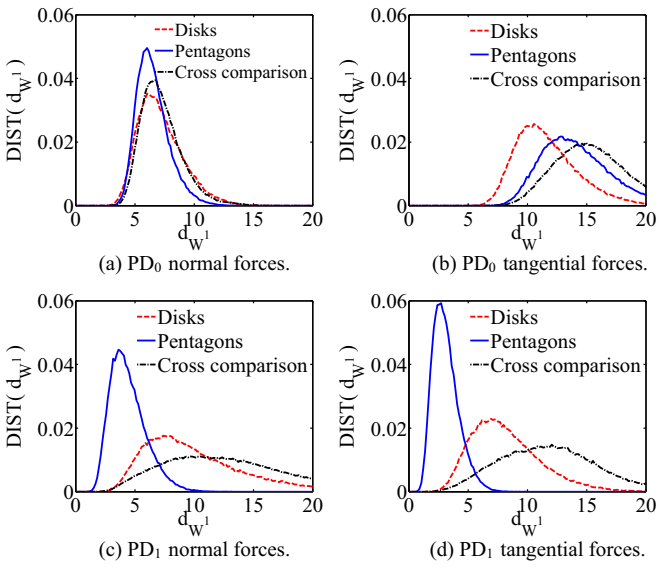

FIG. 13. Distributions of d_{W1} distance (bottom slice, low tapping).

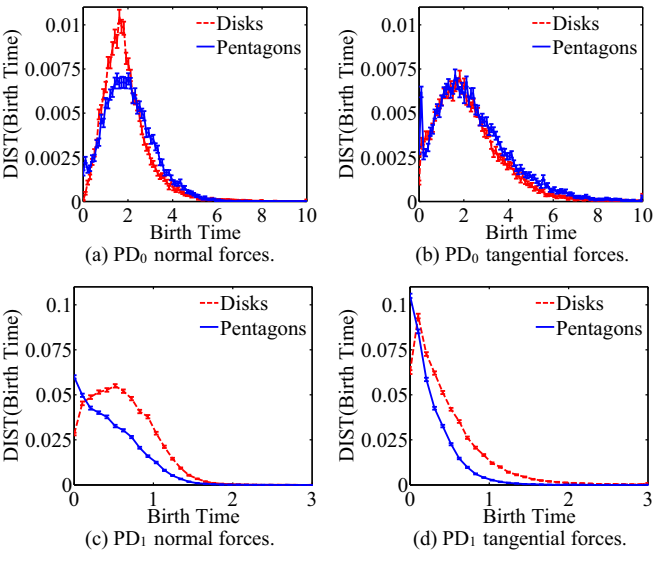

FIG. 15. Distribution of birth times (bottom slice, low tapping). All the features, independent of lifespan, are shown. Compare to Fig. 14 (note different range on the vertical axes).

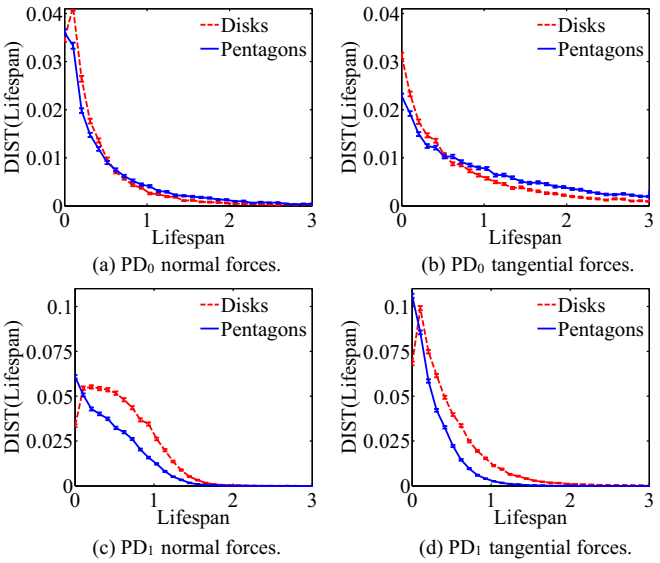

(a) PD_0 normal forces. (b) PD_0 tangential forces. (c) PD_1 normal forces. (d) PD_1 tangential forces.

FIG. 16. Distribution of lifespans (bottom slice, low tapping).

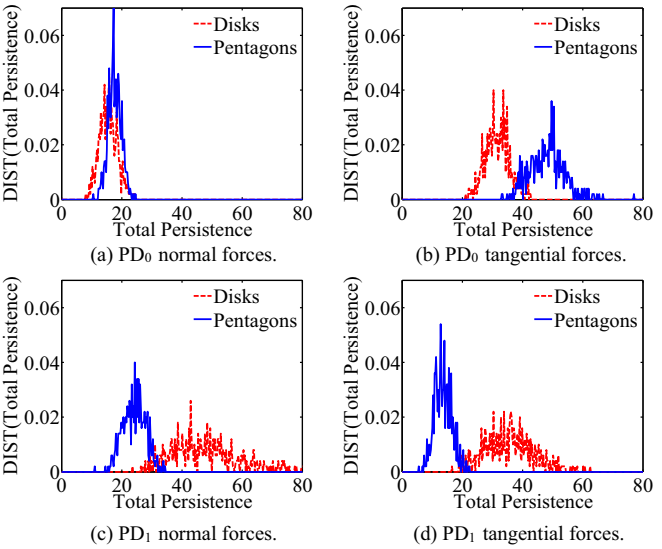

(a) PD_0 normal forces. (b) PD_0 tangential forces. (c) PD_1 normal forces. (d) PD_1 tangential forces.

FIG. 17. Total persistence (bottom slice, low tapping). Note large differences between disks and pentagons.

(b) of Figs. 14 and 15, we do not see much if any difference in the birth times. Regarding loops, the parts (c) and (d) of Figs. 14 and 15, one consistent observation is that there are more points in PDs for disks than for pentagons for the whole range of forces considered. Moreover, for disks, loops start appearing at higher force level than for pentagons. The differences between these two figures show how many of the points have a short lifespan; these differences are particularly interesting for loops, parts (c) and (d) of Figs. 14 and 15: we note a significantly larger number of points for pentagons at small birth times, suggesting that loops for pentagon-based systems form at very small or vanishing force, consistently with the discussion in Ref. [1]. This finding holds both for loops formed by normal and tangential forces.

Figure 16 presents distributions of the lifespans for disks and pentagons. From PD_0 diagrams we conclude that for both disks and pentagons, the dominant number of components is characterized by rather short lifespans. We also observe a cross-over (more pronounced for tangential forces) between disk and pentagon distributions, although the difference is not large. We note that the lifespans larger than ≈ 0.75 are more probable for pentagons than for disks. Therefore, the components live longer for pentagon-based system in particular when tangential forces are considered. To use the landscape analogy, this result says that mountain peaks in the tangential force network are more pronounced for pentagon-based systems. Observe from Figs. 16(c) and 16(d) that the lifespan curves are similar to the birth time curves shown in Fig. 15. This is because for both disks and pentagons, most of the loops disappear very close to the zero force level, and thus the death time provides no additional information.

Figure 17 shows the total persistence, $\mathfrak{T}$, that to a large degree summarizes many of the findings discussed so far. We recall that $\mathfrak{T}$ corresponds to the sum of the lifespans, see Sec. II, so considering the results shown in this figure together with the ones shown in Fig. 16 is useful. For $\mathfrak{T}(PD_0)$ diagrams, there is only a minor difference between disks and pentagons in the normal force network; however, for tangential forces, there are significant differences. This reflects the larger lifespans of the components for pentagon-based system. For $\mathfrak{T}(PD_1)$, the differences are very obvious for both normal and tangential forces, and in contrast to $\mathfrak{T}(PD_0)$ results, here we find that the distribution of $\mathfrak{T}(PD_1)$ is shifted to larger values and is much broader for disk-based systems.

Figure 17 shows clearly significant differences in the structure of force networks in the systems of tapped disks and pentagons. Pentagon systems tend to form new components (clusters) at higher force levels and these endure longer before they merge, in comparison to disk-based ones. This is particularly evident for the tangential force network. In contrast, loops are formed at relatively low force levels in pentagon-based systems. Hence, one could expect that the clusters that form at higher force levels are more stretched (because they do not contain loops) for pentagons. Since most loops persist down to zero force levels, the $\mathfrak{T}(PD_1)$ for pentagons is significantly lower than for disks.

To summarize this section, and more generally the discussion about differences between force networks for disks and pentagons, the main finding is that the force networks differ significantly in their loop structure, although averaged properties, such as those measured by force PDFs do not show any significant difference. Therefore, mechanical responses of the systems built of disks or pentagons, may be very different. Further work will be needed to discuss exactly how different these responses may be, however, already based on the existing results, we expect that the variability of the mechanical responses may be significantly larger for disk-based systems.

IV. CONCLUSIONS

In the present paper, we discuss and describe properties of force networks in tapped particulate systems of disks and pentagons. Our analysis is based on persistent homology that allows us to precisely measure and quantify a number of properties of these networks. The persistence diagrams record the distribution and connectivity of the features (components,

loops) that develop in the force landscape as the force threshold is decreased. These diagrams can then be analyzed and compared by a number of different means, some of them described and used in the present work.

One of the considered concepts is the distance between the persistence diagrams that allows for their direct comparison. The comparison can be carried out on the level of individual diagrams, allowing us to compare between different configurations of nominally the same system, between different parts of a given system, or between completely different systems. In addition, one can compare the distributions of the distances. These comparisons allow us to identify, in a precise manner, the differences between persistence diagrams, and therefore force networks.

In addition to distances, we have defined and used other measures, such as birth times, showing at which force level features appear; lifespans, showing how long the features persist as force threshold is modified; and finally, total persistence, to describe essentially how "mountainous" the force landscape considered is. The listed measures were computed both for components and clusters that could be in a loose sense related to force chains, and for loops that could be related to "holes" in between the force chains.

The use of the outlined measures has allowed us to identify a number of features of force networks. We use these measures, for example, to identify and explain the differences between the systems of disks exposed to different tapping intensities that lead to (on average) the same packing fraction. In addition to identifying the differences between these systems, the implemented measures have also shown that the systems of disks, when exposed to low tapping intensity, evolve in a nontrivial manner, with the subsequent taps possibly correlated to the preceding ones. We have shown that the oscillations in the measures built upon persistence diagrams are correlated with small oscillations in the packing fraction. More generally, the finding is that if the system is tapped strongly and therefore the force network is rebuilt from scratch at each tap, the resulting force networks are similar; however, under low tapping regime, the system (and the resulting force network) appears to be stuck in a certain state and jumps out of it only infrequently. This nontrivial finding and its consequences will be explored in more detail in our future works.

Another comparison that we carried out involves tapped systems of disks and pentagons. One important finding here is that the differences between disks and pentagons are significant when the structure of loops is considered: presence of loops is much more common for the systems of disks than for pentagons, independently of whether normal or tangential forces are considered. On the other hand, the differences between the persistence diagrams based on components and clusters are minor and relatively difficult to identify. Therefore, the force networks that form in tapped systems of disks and pentagons are similar when only components are considered, but significantly different when loops are included.

The comparison between the networks can be done on the level of individual realizations, and on the level of averaged properties. When considering the importance of the results to the macro-scale response, both approaches are relevant. For example, the fact that the distances, that measure the variability of networks between realizations, differ significantly between disks and pentagons, shows that the response of a pentagon based system (determined by the force network properties) to external perturbation is much more predictable, compared to the response of disks. Considering averaged responses shows again significant differences between disks and pentagons, particularly for tangential forces, and for loop structure. This different averaged connectivity of force networks, shows clearly that different response of the system as a whole to externally imposed perturbation is expected. To quantify more precisely the connection between the properties of force networks and macroscopic response, it will be necessary to consider in a coordinated study the properties of force networks and the response itself, and develop correlation between the both. Persistence analysis clearly provides sufficient information to carry out such a study. This new information opens the door for developing more elaborate comparisons, measures, and also connections between the force network properties and mechanical response of a system at the macroscale. Furthermore, the analysis that we presented here can be easily applied to the three dimensional systems, where any direct visualization may be difficult. Our future research will proceed in this direction.

ACKNOWLEDGMENTS

K.M. and M.K. were partially supported by NSF Grants No. DMS-0915019, No. 1125174, and No. 1248071, and contracts from AFOSR and DARPA. L.K. acknowledges support by NSF Grants No. DMS-0835611 and No. DMS-1521717.

[1] L. A. Pugnaloni, C. M. Carlevaro, M. Kramár, K. Mischaikow, and L. Kondic, Phys. Rev. E **93**, 062902 (2016).
[2] R. Arévalo, L. A. Pugnaloni, I. Zuriguel, and D. Maza, Phys. Rev. E **87**, 022203 (2013).
[3] M. Kramár, A. Goullet, L. Kondic, and K. Mischaikow, Phys. Rev. E **87**, 042207 (2013).
[4] M. Kramár, A. Goullet, L. Kondic, and K. Mischaikow, Phys. Rev. E **90**, 052203 (2014).
[5] M. Kramár, A. Goullet, L. Kondic, and K. Mischaikow, Physica D **283**, 37 (2014).
[6] A. Tordesillas, D. M. Walker, and Q. Lin, Phys. Rev. E **81**, 011302 (2010).
[7] D. S. Bassett, E. T. Owens, K. E. Daniels, and M. A. Porter, Phys. Rev. E **86**, 041306 (2012).
[8] M. Herrera, S. McCarthy, S. Slotterback, E. Cephas, W. Losert, and M. Girvan, Phys. Rev. E **83**, 061303 (2011).
[9] D. M. Walker and A. Tordesillas, Phys. Rev. E **85**, 011304 (2012).
[10] D. S. Bassett, E. T. Owens, M. A. Porter, M. L. Manning, and K. E. Daniels, Soft Matter **11**, 2731 (2015).

[11] M. Kramár, R. Levanger, J. Tithof, B. Suri, M. Xu, M. Paul, M. Schatz, and K. Mischaikow, Phys. D (to be published).
[12] Y. Mileyko, S. Mukherjee, and J. Harer, Inverse Problems **27**, 124007 (2011).
[13] E. Munch, K. Turner, P. Bendich, S. Mukherjee, J. Mattingly, and J. Harer, Electron. J. Statist. **9**, 1173 (2015).
[14] P. Bubenik, J. Mach. Learn. Res. **16**, 77 (2015).
[15] M. Kramár (2012), http://math.rutgers.edu/miroslav/Sowftware.html.
[16] V. Nanda (2012), http://www.math.rutgers.edu/vidit/perseus.html.
[17] U. Bauer, M. Kerber, J. Reininghaus, and H. Wagner, in *Mathematical Software–ICMS 2014* (Springer, Berlin/Heidelberg, 2014), pp. 137–143.